Mathematical modeling of metal ion homeostasis and signaling systems

Cui, J.

Publication date
2009

Chapter 4 Simulating Complex Calcium-Calcineurin Signaling Networks in Cardiac Myocytes[12]

4.1 Introduction:

As mentioned in Section 1.3.4.1, it has been recently recognized that calcium plays a central role in the control of heart growth through a complex calcium-calcineurin-MCIP-NFAT signaling network (see Fig. 4.1). The heart responds to physiological and pathological stimuli by hypertrophic growth [224, 225]. Cardiac hypertrophy is a thickening of the heart muscle (myocardium) resulting in a decrease in size of the ventricles. Prolonged pathological hypertrophy may progress to heart failure and significantly increase the risk for sudden death. Thus deciphering the details of the signaling pathways involved in cardiac hypertrophy and understanding their quantitative dynamics through computational modeling will be critical for devising therapeutic drugs for the treatment of heart disease [225].

[12] This Chapter is based on: Jiangjun Cui and Jaap Kaandorp, Simulating complex calcium-calcineurin signaling network, in M.T. Bubak; G.D. van Albada; J.J. Dongarra and P.M.A. Sloot, editors, *Computational Science - ICCS 2008: 8th International Conference, Krakow, Poland, Proceedings, Part III*, in series *Lecture Notes in Computer Science*, vol. 5103, pp. 110-119. Springer, Berlin, Heidelberg, June 2008.

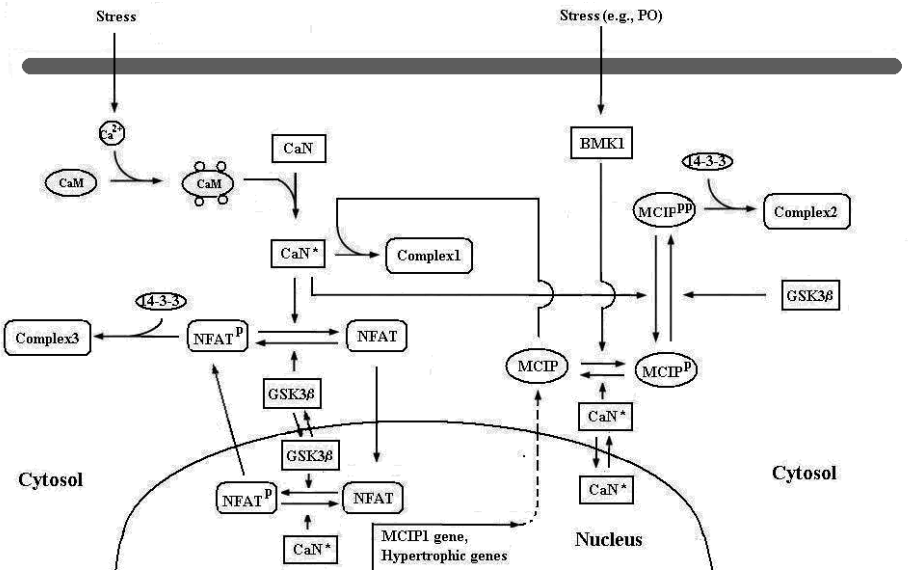

Figure. 4.1. A schematic graph depicting the Ca^{2+}-calcineurin-MCIP-NFAT signaling networks in cardiac myocytes.[13]

As shown in the left-up corner of Fig. 4.1, stress incurs the influx of Ca^{2+}, which binds to CaM (4:1). Ca^{2+}-bound CaM binds to CaN to activate it [175]. CaN^* (i.e., activated CaN) can bind to MCIP to form Complex1 [225,226]. CaN^* can also work as the enzyme to convert $NFAT^P$ into NFAT [148]. Another enzyme GSK3β works in the reverse conversion of NFAT into $NFAT^P$, which can bind to 14-3-3 to form Complex3 [13,130]. Such conversion between NFAT and $NFAT^P$ with the help of two enzymes (GSK3β and CaN^*) also happen in the nucleus [91]. NFAT in the cytosol will be imported into the nucleus and $NFAT^P$ in the nucleus will be exported into the cytosol. The nuclear NFAT can initiate the transcription of the hypertrophic genes and the gene encoding MCIP (more precisely, MCIP1, a form of MCIP) [91,239]. Both GSK3β and CaN^* are shuttled between the nucleus and the cytosol [91, 183]. As shown in the right-up corner of Fig. 4.1, particular stress such as PO can activate BMK1 [214], which catalyzes the conversion of

[13] Abbreviations are as follows: calmodulin (CaM); calcineurin (CaN); activated calcineurin (CaN^*); nuclear factor of activated T-cells (NFAT); phosphrylated NFAT($NFAT^P$); modulatory calcineurin-interacting protein (MCIP); phosphorylated MCIP on serine 112 ($MCIP^P$); phosphorylated MCIP on both serine 112 and serine 108 ($MCIP^{PP}$); big mitogen-activated protein kinase 1 (BMK1); glycogen synthase 3β (GSK3β); the complex formed by MCIP and calcineurin(Complex1); the complex formed by $MCIP^{PP}$ and 14-3-3 (Complex2); the complex formed by $NFAT^P$ and 14-3-3 (Complex3); pressure overload (PO); hypertrophic stimuli (stress).

MCIP into $MCIP^P$ [1], $MCIP^P$ can be converted into $MCIP^{PP}$ by GSK3β. The reverse conversion of $MCIP^{PP}$ into $MCIP^P$ is again catalyzed by CaN^* [226]. $MCIP^{PP}$ will bind with 14-3-3 to form Complex2 [1].

MCIP1 seems to facilitate or suppress cardiac CaN signaling depending on the nature of the stress (see Fig. 4.2a). In the case of CaN^* transgenic mice, the knock-out of MCIP1 gene (i.e., MCIP $^{-/-}$ TG mice) exacerbated the hypertrophic response to CaN^* overexpression. Paradoxically, however, cardiac hypertrophy in response to PO was blunted in normal MCIP $^{-/-}$ mice [101,225].

In 2006, Shin *et al*. [196] published a paper in FEBS Letters using switching feedback mechanism to explain this dual role of MCIP in cardiac hypertrophy. The aim of this Chapter is to propose a much-extended version of Shin's model by including more recent experimental findings. The construction of the model is based on biochemical principles and we use an open source software (Cellerator) to automatically generate the equations. As we will see later, this model can correctly predict the mutant ($MCIP1^{-/-}$) behavior under different stress such as PO and CaN^* overexpression.

4.2 Method:

4.2.1 Cellerator Software

Cellerator™ is a Mathematica® package designed to facilitate biological modeling via automated equation generation [194, 245]. It uses an arrow-based reaction notation to represent biochemical networks and is especially amenable for simulating signal transduction networks.

For example, a catalytic biochemical reaction ($S+E \underset{r2}{\overset{r1}{\rightleftharpoons}} SE \xrightarrow{r3} P+E$, which means enzyme E catalyzes the conversion of S into P, where r1, r2, r3 are the rate constants and SE is the intermediate complex formed by S and E [58]) can be represented as $\left\{S \overset{E}{\rightleftharpoons} P,\ r1,\ r2,\ r3\right\}$ in Cellerator form. The detailed ODEs notation of this reaction are:

$$\frac{dS}{dt} = -r1 * E * S + r2 * SE, \frac{dP}{dt} = r3 * SE, \frac{dE}{dt} = -\frac{dSE}{dt} = -r1 * E * S + (r2 + r3) * SE$$

In our system shown in Fig. 4.1, the conversion of MCIP into $MCIP^P$ catalyzed by BMK1 can be represented as $\left\{MCIP \overset{BMK1}{\rightleftharpoons} MCIPp,\ k7,\ k8,\ k9\right\}$ in Cellerator form where MCIPp denotes $MCIP^P$ and $k7$, $k8$, $k9$ are the relevant rate constants.

4.2.2 Representation of Relevant Reactions

The complex Ca^{2+}-calcineurin signaling network shown in Fig. 4.1 can be represented using 17 reactions in addiction to a transcription control process of MCIP by NFAT. For clarity, we can group all 17 relevant reactions into four categories (simple irreversible,

simple reversible, reversible binding and catalytic binding reactions) which are shown in the following Table 4.1.

Table 4.1: The Representation of relevant reactions of the system [14]

Reaction Category	Biochemical Form	Cellerator Form	Reaction No.	Cellerator Form of Particular Reactions
Simple Irreversible	$A \xrightarrow{r} B$	{A → B, r}	(1)	{NFATc → NFATn, k29}
			(2)	{NFATpn → NFATpc, k30}
Simple Reversible	$A \underset{r2}{\overset{r1}{\rightleftharpoons}} B$	{A ⇄ B, r1, r2}	(3)	{GSK3βc ⇄ GSK3βn, k31, k32}
			(4)	{CaNc* ⇄ CaNn*, k33, k34}
Reversible Binding	$A+B \underset{r2}{\overset{r1}{\rightleftharpoons}} C$	{A+B ⇄ C, r1, r2}	(5)	{CaM + Ca^4 ⇄ CaMCa, k1, k2}
			(6)	{CaMCa + CaNc ⇄ CaNc*, k3, k4}
			(7)	{CaNc* + MCIP ⇄ Comp1, k5, k6}
			(8)	{P1433 + MCIPpp ⇄ Comp2, k19, k20}
			(9)	{NFATpc + P1433 ⇄ Comp3, k27, k28}
Catalytic Binding	$S+E \underset{r2}{\overset{r1}{\rightleftharpoons}} SE$ $SE \xrightarrow{r3} P+E$	$\left\{S \overset{E}{\rightleftarrows} P, r1, r2, r3\right\}$	(10)	$\left\{MCIP \overset{BMK1}{\rightleftarrows} MCIPp, k7, k8, k9\right\}$
			(11)	$\left\{MCIPp \overset{CaNc^*}{\rightleftarrows} MCIP, k10, k11, k12\right\}$
			(12)	$\left\{MCIPp \overset{GSK3\beta c}{\rightleftarrows} MCIPpp, k13, k14, k15\right\}$
			(13)	$\left\{MCIPpp \overset{CaNc^*}{\rightleftarrows} MCIPp, k16, k17, k18\right\}$
			(14)	$\left\{NFATpc \overset{CaNc^*}{\rightleftarrows} NFATc, k21, k22, k23\right\}$
			(15)	$\left\{NFATc \overset{GSK3\beta c}{\rightleftarrows} NFATpc, k24, k25, k26\right\}$
			(16)	$\left\{NFATpn \overset{CaNn^*}{\rightleftarrows} NFATn, k35, k36, k37\right\}$
			(17)	$\left\{NFATn \overset{GSK3\beta n}{\rightleftarrows} NFATpn, k38, k39, k40\right\}$

[14] Abbreviations and synonyms used in this table are as follows: $MCIP^P$ (MCIPp); $MCIP^{PP}$ (MCIPpp); $NFAT^P$ (NFATp); cytosolic NFAT (NFATc); cytosolic NFATp (NFATpc); cytosolic inactive CaN (CaNc); cytosolic CaN^* ($CaNc^*$); cytosolic GSK3β (GSK3βc); nuclear NFAT (NFATn); nuclear NFATp (NFATpn); nuclear CaN^* ($CaNn^*$); nuclear GSK3β (GSK3βn); 14-3-3 protein (P1433); Ca^{2+}-bound CaM (CaMCa); Complex1 (Comp1); Complex2 (Comp2); Complex3 (Comp3).

4.2.3 The Equations of the Model

The model consists of 28 equations concerning 28 unknowns including $Ca(t)$ which denotes the cytosolic Ca^{2+} concentration. Since calcineurin is unique in its specific responsiveness to sustained, low frequency calcium signals [224], we will assume cytosolic Ca^{2+} concentration as a constant in the following simulations as Shin *et al.* [196] did in their simulations. Then we need to further consider modeling the transcription control process of MCIP by NFAT. We have added the following equation to replace the equation of $Ca(t)$ in our model:

$$\frac{dMRNA(t)}{dt} = k41 * NFATn(t) - k42 * MRNA(t) \tag{4.1}$$

Where $MRNA(t)$ denotes the mRNA concentration of MCIP and $k41$ is the control constant, $k42$ is the degradation constant [242]. Moreover, we need to add an additional production term ($k43 * MRNA(t)$) and a degradation term ($(\ln 2 / t_{1/2}) * MCIP(t)$) in the rate equation of $MCIP(t)$ where $t_{1/2}$ denotes the half-life time constant of MCIP. Thus eventually we have completed building of our computational model which consists of 28 ODEs for 28 unknowns. The relevant parameters except parameter Ca ,which denotes cytosolic calcium concentration, are listed in Table 4.2.

Table 4.2: Rate constants and other parameters of the model[15]

Parameters	Value		Parameter	Value
$k1$	5 $\mu M^{-4} \cdot min^{-1}$		$k24$	0.1 $\mu M^{-1} \cdot min^{-1}$
$k2$	100 min^{-1}		$k25$	0.15 min^{-1}
$k3$	2760 $\mu M^{-1} \cdot min^{-1}$ [175]		$k26$	0.1 min^{-1}
$k4$	0.072 min^{-1} [175]		$k27$	0.4 $\mu M^{-1} \cdot min^{-1}$
$k5$	50 $\mu M^{-1} \cdot min^{-1}$		$k28$	0.1 min^{-1}
$k6$	0.0567 min^{-1} [196]		$k29$	0.4 min^{-1} [183]
$k7$	5 $\mu M^{-1} \cdot min^{-1}$		$k30$	0.1 min^{-1} [183]
$k8$	0.1 min^{-1}		$k31$	0.1 min^{-1}

[15] In this table, $t_{1/2}$ denotes the half-life time of MCIP1. $[CaN_{tot}]$ denotes total concentration of calcineurin. $[NFAT_{tot}]$ denotes total concentration of NFAT.

$k9$	0.5 min^{-1}		$k32$	0.05 min^{-1}
$k10$	0.1 $\mu M^{-1} \cdot min^{-1}$		$k33$	0.114 min^{-1} [195]
$k11$	0.1 min^{-1}		$k34$	0.0552 min^{-1} [195]
$k12$	0.1 min^{-1}		$k35$	0.15 $\mu M^{-1} \cdot min^{-1}$
$k13$	0.5 $\mu M^{-1} \cdot min^{-1}$		$k36$	0.1 min^{-1}
$k14$	0.5 min^{-1}		$k37$	0.2 min^{-1}
$k15$	0.1 min^{-1}		$k38$	0.1 $\mu M^{-1} \cdot min^{-1}$
$k16$	0.1 $\mu M^{-1} \cdot min^{-1}$		$k39$	0.1 min^{-1}
$k17$	0.1 min^{-1}		$k40$	0.1 min^{-1}
$k18$	0.1 min^{-1}		$k41$	0.02 min^{-1}
$k19$	0.5 $\mu M^{-1} \cdot min^{-1}$		$k42$	0.03 min^{-1}
$k20$	0.1 min^{-1}		$k43$	0.03 min^{-1}
$k21$	0.15 $\mu M^{-1} \cdot min^{-1}$		$t_{1/2}$	15 min [177]
$k22$	0.15 min^{-1}		$[CaN_{tot}]$	1 μM [24,196]
$k23$	0.1 min^{-1}		$[NFAT_{tot}]$	0.017 μM [15,196]

The initial condition used for the simulations is as follows (Units are in μM):

$$BMK1(0) = 0.012, MRNA(0) = 3.33*10^{-4}, CaM(0) = 25.2, CaMCa(0) = 7.88*10^{-7},$$
$$CaNc(0) = 0.91, CaNc^{*}(0) = 0.0275, CaNn^{*}(0) = 0.0568, Comp1(0) = 5.21*10^{-3},$$
$$Comp2(0) = 0.283, Comp3(0) = 0.014, GSK3\beta c(0) = 0.17, GSK3\beta n(0) = 0.339,$$
$$MCIP(0) = 2.15*10^{-4}, MCIPp(0) = 7.76*10^{-3}, MCIPpp(0) = 0.0798, P1433(0) = 0.708,$$
$$NFATc(0) = 2*10^{-5}, NFATn(0) = 4.99*10^{-4}, NFATpc(0) = 4.94*10^{-3}, NFATpn(0) = 8.01*10^{-5},$$
$$NFATc \cup GSK3\beta c(0) = 1.36*10^{-6}, NFATn \cup GSK3\beta n(0) = 8.46*10^{-5},$$
$$MCIPp \cup GSK3\beta c(0) = 1.1*10^{-3}, MCIP \cup BMK1(0) = 2.14*10^{-5},$$
$$MCIPpp \cup CaNc^{*}(0) = 1.1*10^{-3}, MCIPp \cup CaNc^{*}(0) = 1.07*10^{-4},$$
$$NFATpn \cup CaNn^{*}(0) = 2.27*10^{-6}, NFATpc \cup CaNc^{*}(0) = 8.15*10^{-5}$$

It is easy to verify that this initial conditions satisfies the constraints of $[NFAT_{tot}] = 0.017\mu M$ and $[CaN_{tot}] = 1\mu M$. (Please note that here $MCIP \cup BMK1(0)$ denotes the initial concentration of intermediate complex formed by MCIP and BMK1).

4.3 Results

With this model, the next question is how to simulate the stimulus. Similar as Shin *et al.* did in their paper, we simulate stimulus of PO by setting parameter Ca to a smaller constant (0.2μM). Moreover, at the same time we increase the initial value of $BMK1(t)$ from 0.012μM to 1.2 μM because PO activates BMK1 [214]. The stimulus of CaN^{*} overexpression is simulated by setting parameter Ca to a bigger constant (0.4μM) and simultaneously increasing the initial value of $CaNc^{*}(t)$ from 0.0275μM to 0.825 μM.

4.3.1 Steady-state Property

By numerically solving the equations using the parameters listed in Table 4.2, simulations show that the system does evolve to a steady state. Actually the above initial condition is a selected steady state for simulating the normally growing heart cells with parameter $Ca = 0.05\mu M$. In Fig. 4.2b, the steady-state value increase of nuclear NFAT (i.e., $NFATn^{*}(t)$) under the different stimuli for simulated $MCIP^{+/+}$ and $MCIP^{-/-}$ heart cells are shown. By comparison of the first two bars in this figure, we can see that PO causes greater increase of the steady-state value of nuclear NFAT in simulated normal cells than in simulated MCIP mutant cells. However, the comparison of the third bar with the fourth bar tells us that CaN^{*} overexpression incurs much less increase of the steady state value of nuclear NFAT in simulated normal cells than in simulated $MCIP^{-/-}$ cells.

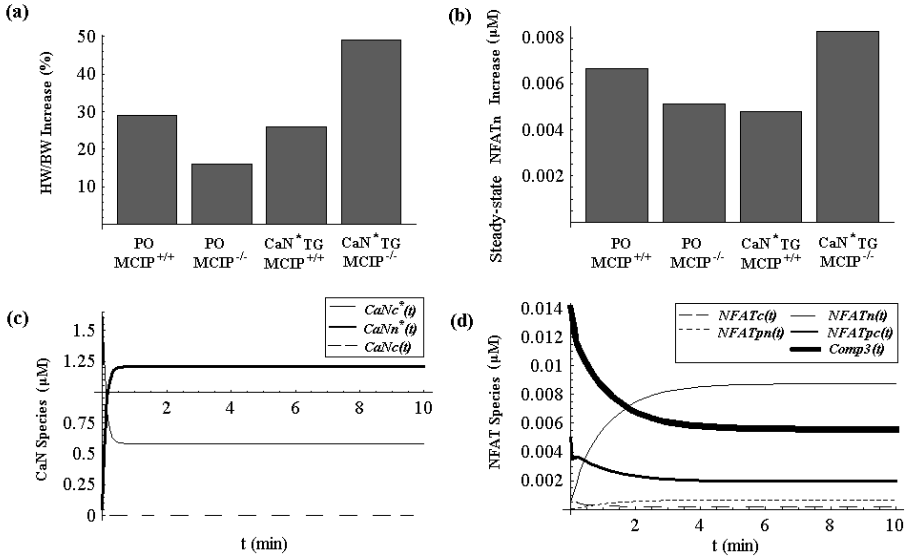

Figure. 4.2. Hypertrophic response and simulated transient curves for CaN* TG animals. (a) The stimuli of pressure overload (PO) caused more severe hypertrophy in normal animals (the first bar) than in MCIP$^{-/-}$ animals (the second bar) whereas the stimuli of CaN* overexpression (expressed from a muscle-specific transgene) incurred much more HW/BW (heart weight normalized to body weight) increase in MCIP$^{-/-}$ transgenic (TG) mice (the fourth bar) than in normal transgenic mice (the third bar). (b) The simulated value increase of steady-state nuclear NFAT under the different stimuli of PO and CaN* overexpression. (c) Simulated CaN species concentration as a function of t in the case of CaN* overexpression for MCIP$^{-/-}$ animals. Thin solid line: $CaNc^*(t)$; thick solid line: $CaNn^*(t)$; Dashed line: $CaNc(t)$. (d) Simulated NFAT species concentration as a function of t in the case of CaN* overexpression for MCIP$^{-/-}$ animals. Thin solid line: $NFATn(t)$; thick solid line: $NFATp(t)$; extremely thick solid line: $Comp3(t)$;sparsely dashed line: $NFATc(t)$; densely dashed line: $NFATpn(t)$.

4.3.2 Transients and Mutant behavior

In Fig. 4.3, critical transient curves in the case of CaN* overexpression for simulated MCIP$^{+/+}$ cells are shown. From Fig. 4.3a, we can see that due to overexpression, cytosolic CaN* quickly (in less than 4 minutes) rises to high peak of 1.3 μM, drops a bit more slowly to around 0.6 μM and then very gradually declines (it eventually rests at a level of 0.353 μM). From Fig. 4.3b, we can see that the concentration of MCIP^{PP} gradually decreases from 0.0798 μM to almost 0, whereas the concentration of MCIP^{P} rapidly rises to a peak value of 0.036 μM and then gradually declines. From Fig. 4.3c, we can see that the concentration of Complex2 gradually declines from 0.283 μM to a resting level of 0.025 μM whereas the concentration of Complex1 increases from almost 0 to around 0.5 μM in 50 hours (it will eventually rests at 0.71 μM). The concentration of 14-3-3 gradually rises from 0.71 μM to 0.97 μM. From Fig. 4.3d, we can see that the concentration of nuclear NFAT quickly rises to a peak value of 7.6 nM and then gradually declines (it will eventually rests at 5.3 nM) whereas cytosolic NFATp

decreases quickly from 4.9 nM to 2 nM and then gradually recovers to a new resting level of 2.5 nM. The concentration of Complex3 quickly decreases from 14nM to 7nM and then gradually recovers to 7.1nM.

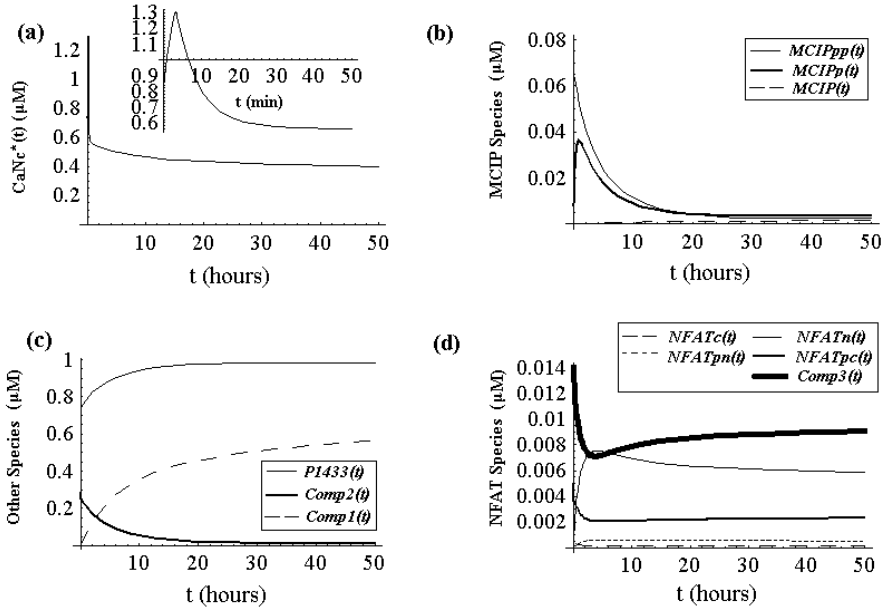

Figure. 4.3. Simulated transient curves for normal animals under the stimulus of CaN* overexpression. (a) Simulated $CaNc^*(t)$ (i.e., cytosolic CaN*) as a function of t. The small figure in the right-up corner shows the detailed change of $CaNc^*(t)$ during the first 50 minutes. (b) Simulated concentration of MCIP species as a function of t. Thin solid line: $MCIPpp(t)$; thick solid line: $MCIPp(t)$; dashed line: $MCIP(t)$; (c) Simulated concentration of some other species as a function of t. Thin solid line: $P1433(t)$; thick solid line: $Comp2(t)$; dashed line: $Comp1(t)$. (d) Simulated NFAT species concentration as a function of t. Thin solid line: $NFATn(t)$; thick solid line: $NFATpc(t)$; extremely thick solid line: $Comp3(t)$;sparsely dashed line (bottom): $NFATc(t)$; densely dashed line: $NFATpn(t)$.

Similarly, we can perform numerical simulations for the MCIP$^{-/-}$ animals. Fig. 4.2c and Fig. 4.2d show the transient curves of the main CaN species and NFAT species under the stimulus of CaN* overexpression. From Fig. 4.2c, we can see that due to CaN* overexpression, cytosolic inactive CaN (i.e., $CaNc(t)$) quickly decreases from 0.091 μM to 0 and cytosolic CaN* rises extreme quickly (actually in less than 0.01 minutes) from 0.825 μM to high peak of more than1.6 μM and then quickly declines to a resting level of 0.58 μM whereas nuclear CaN* quickly rises from 0.057 μM to 1.21 μM. From Fig. 4.2d, we can see that nuclear NFAT steadily increases from 0.5nM to a resting level of 8.8 nM whereas cytosolic NFATp extreme quickly drops from 4.9 nM to 3.8 nM and then gradually declines to 1.9nM.

4.4 Discussion

The decrease of Complex2 shown in Fig. 4.3C indicates the accelerated dissociation of Complex2 which should produce more $MCIP^{PP}$ (see Reaction 8 in Table 4.1). However, from Fig. 4.3b, we can see that $MCIP^{PP}$ is actually decreasing. Since only two reactions (Reaction 8 and 13) can cause the decrease of $MCIP^{PP}$, so the only feasible explanation is that the initial sudden rise of cytosolic CaN^{*} catalyzes the conversion of $MCIP^{PP}$ to $MCIP^{P}$ and then to MCIP and the resultant depletion of $MCIP^{PP}$ promotes the dissociation of Complex2 which also causes the concentration rise of 14-3-3 as seen in Fig. 4.3c. Similarly, the sudden decrease of Comp3 should release more $NFAT^{P}$ (see Reaction 9 in Table 4.1). However, as we can see from Fig. 4.3d, $NFAT^{P}$ concentration is at first rapidly decreasing. So the only feasible explanation is the initial sudden rise of cytosolic CaN^{*} catalyzes the conversion of cytosolic $NFAT^{P}$ to NFAT and the resultant depletion of cytosolic $NFAT^{P}$ promotes the dissociation of Complex3. The accelerated cytosolic $NFAT^{P}$ to NFAT also results in the translocation of NFAT into the nucleus which explains the increases of nuclear NFAT which will promotes the expression of MCIP. The increasing formation of Complex1 shown in Fig. 4.3c indicates that the MCIP converted from $MCIP^{P}$ and the newly expressed MCIP associate with cytosolic CaN^{*}, which leads to its depletion as shown in Fig. 4.3a (obviously the intial rise of cytosolic CaN^{*} concentration in the first several minutes is due to the increased level of cytosolic Ca^{2+} which binds with calmodulin to further activate cysolic CaN). Since in first 50 hours, the total increase of Complex1 concentration (about 0.5 μM) is greater than the total decrease (less than 0.4 μM) of the concentrations of three MCIP species shown in Fig. 4.3b and Complex2, we can conclude that a significant source of MCIP consumed in the process of increasing formation of Complex1 is from newly expressed MCIP. The increasing formation of Complex1 also consumes cytosolic CaN^{*} and realizes the inhibition of MCIP on calcineurin (CaN) activity. In simulated MCIP $^{-/-}$ cells, due to the lack of MCIP, nuclear NFAT increases to a much higher level (8.8nM) than in MCIP $^{+/+}$ cells (5.3 nM) as shown in Fig. 4.2d. Also it takes much less time for the system to evolve to new steady state.

Similarly, the simulations in the case of PO stimulus show that in normal cells, PO causes the increase of Comlex2 formation (from 0.28 μM to 0.96 μM) and the decrease of free 14-3-3 concentration (from 0.71 μM to 0.048 μM). The formation of Complex2 consumes $MCIP^{PP}$ and promotes the conversion of MCIP to $MCIP^{P}$ then to $MCIP^{PP}$. In simulated MCIP $^{-/-}$ cells, due to the existence of large quantity of free 14-3-3, nuclear NFAT increases from 0.5 nM to a less higher level (5.6 nM) than in MCIP $^{+/+}$ cells (7.2 nM) as shown in Fig. 4.2b.

By comparison of the experimental and simulated hypertrophic response to different stimuli shown in Fig. 4.2a and Fig. 4.2b, we can see both two second bars are lower than the corresponding first bars, which means that our model does reproduce the seemingly facilitating function of MCIP on hypertrophic response under the stimuli of PO. Moreover, The two fourth bars are higher than the corresponding third bars which means

that our model does reproduce the inhibitory function of MCIP on hypertrophic response under the stimuli of CaN^* overexpression.

Finally there is still an issue worth discussion. In the current model, we assume that CaN^* overexpression causes the simultaneous increase of cytosolic calcium concentration and the increase of cytosolic active calcineurin concentration. In the real case, there will be some time difference (typically several minutes) between these two events. After including a time delay into our model accounting for this time difference, further investigations show that although the simulated dynamics (especially the short term dynamics of $CaNc^*(t)$) shows some difference, the steady state value of simulated nuclear NFAT concentration remains the same. Similar is the case for the simulations for PO stimulus.

To summarize, we have built a computational model for the complex calcium-calcineurin-MCIP-NFAT signaling network in cardiac myocytes. Our model can correctly predict the mutant ($MCIP^{-/-}$) behavior under different stress such as PO and CaN^* overexpression (compare Fig. 4.2b with Fig. 4.2a). Our simulation results suggest that in the case of PO, the seemingly facilitating role of MCIP is due to activated BMK1 that promotes the conversion of MCIP to $MCIP^P$ and then to $MCIP^{PP}$ which associates with 14-3-3 to relieve the inhibitory effect of 14-3-3 on hypertrophic response. In the case of CaN^* TG mice, the overexpressed CaN^* causes the dissociation of Complex2 by promoting the conversion of $MCIP^{PP}$ to $MCIP^P$ then to MCIP, which associates with CaN^* to inhibit its activity. Moreover, the feedback loop of MCIP expression controlled by NFAT contributes significantly to this inhibition.

In this chapter and previous two chapters, we presented several mathematical models for calcium homeostasis and signaling systems in yeast cells and mammalian cardiac myocytes. As mentioned in Section 1.3.4.7, similar as Ca^{2+}, Zn^{2+} also functions as an important signaling molecule in various organisms. In Chapter 5, we will present a mathematical model developed for simulating the *in vitro* transcriptional response of zinc homeostasis in *E. coli*.